Surface Science 87 (1979) 683–699

THEORY OF ION SCATTERING FROM SINGLE CRYSTALS

Barbara J. GARRISON *

Department of Chemistry, The Pennsylvania State University, University Park, Pennsylvania 16802, USA

Received 18 January 1979; manuscript received in final form 4 May 1979

The scattering of He^+, Ne^+ and Ar^+ ions at 600 eV from Ni(110) in the [1$\bar{1}$0] direction is modeled using classical dynamics. The distributions of final scattering angles of the primary ions are displayed as contour plots over the surface impact zone. From the contour plots the regions of the surface that give rise to scattering at specific angles can be isolated. The majority of the inplane scattering arises from collisions of the primary ion with second layer or "valley" atoms. However, to correctly reproduce the experimental energy distribution curves of Heiland and Taglauer (J. Vacuum Sci. Technol. 9 (1971) 620), we must include a simple collision time correction to account for neutralization of the ion beam. This analysis predicts that the ions which collide with second layer atoms of the solid are preferentially neutralized. The energy distributions due to first layer collisions agree well with experiment. We find that a full molecular three dimensional model is needed to describe all of the ion scattering events since for most of the collisions, the ion is simultaneously interacting with at least two atoms of the solid. However, in agreement with other workers we find only a single collision is responsible for the "binary" peak in the energy distribution. In addition the relative scattering intensity at different angles is dependent on having a three-dimensional solid.

1. Introduction

The characterization of solid surfaces by ion beams has been the focus of researchers over the past decade. The details of the surface structure are inferred either by measuring the energy and angular distributions of the scattered primary ion beam or by analyzing the ejected particles for yields, cluster formation, energy and angular distributions. Of interest for this study is the characterization of the constituents and structure of a surface by scattering of ion beams. This technique for primary ions in the range of ~500–5000 eV is often called ion scattering spectrometry (ISS) or low energy ion scattering (LEIS). The energy distribution of the reflected ions yields peaks which are characteristic of the mass of the target elements. For some adsorbate systems, it appears that the angular distributions yield structural information. The relative positions of some species shadow or block other species from scattering the primary ion.

* Work performed at Purdue University, West Lafayette, Indiana 47907, USA.

Several models for the scattering of ions from a surface have been proposed [1]. Virtually all of the models employ the binary collision approximation (BCA) [2]; that is, the ion only interacts with *one* atom in the solid at a time. This approximation has been used with a one-atom solid [3], a two-atom solid [4], a chain of atoms [5] and a three-dimensional solid [6]. To our knowledge only one group has included the simultaneous interactions of the ion with all the surface atoms, but this calculation was only completed for 13 impact parameters of the incident ion [7]. The models work reasonably well in describing the scattering characteristics of clean metal single crystals. In this work we use a three-dimensional model, which includes not only the interactions between the primary ion and the solid, but also interactions among the atoms of the solid, to describe the ion scattering process. The purpose in developing this model is to gain a thorough understanding of the collision mechanisms that are important in low energy ion scattering. Ultimately we wish to analyze more complicated systems such as alloys or adsorbates on surfaces where the scattering events are more complex. In the spirit of trying to understand the basic processes involved, thermal effects will be omitted, since they complicate the computation and analysis, while only broadening the energy distribution peaks. It is possible, however, to include thermal effects in this model.

In this paper the scattering of He^+, Ne^+ and Ar^+ ions at 600 eV from nickel (110) in the $[1\bar{1}0]$ direction is modeled using classical dynamics. The solid consists of 2–3 layers with a total of 18–30 atoms. The results of the full molecular dynamics treatment are compared to the experimental results of Heiland and Taglauer [8]. We find that ions both reflecting from the "ridge" or first layer atoms and from the "valley" or second layer atoms contribute to inplane scattering. However, to correctly reproduce the experimental energy distribution curves we must include a simple collision time correction to account for neutralization of the ion beam. Although more than half of the in-plane scattering comes from second layer effects (surface semi-channeling), these ions are preferentially neutralized so that the observed energy distributions are due to first layer collisions. The energy distributions due to first layer collisions agree well with the experimental curves.

We find that a full three-dimensional model is necessary as many of the collisions, particularly along the second layer, are not well approximated using the BCA. Also a considerable width to the impact region along the ridge gives rise to in-plane scattering which alters the intensity vs. angle from what a two-dimensional chain model would predict.

2. Description of the calculation

The ion bombardment process is followed by integrating Hamilton's equations of motion for the ion–solid system. This procedure is similar to our previous model for SIMS (secondary ion mass spectrometry) except that in the SIMS model we are interested in the particles that eject from the solid [9] and here we analyze the

reflected primary ion. For the ejection process the infinite solid is approximated by a crystallite of 4 layers of 60 atoms each. Crystal size testing shows that the crystallite must have at least ~240 atoms to contain the majority of the ejection events [9]. In the ion scattering calculations, since we are not interested in the subsequent motion of the atoms of the solid, we find that a crystallite of 18–30 atoms is sufficient to describe the scattering of the primary ion. The surface size necessary to accurately calculate the primary ion trajectory for Ni(110) is shown in fig. 1. For He^+ and Ne^+ scattering, 2 layers (18 atoms) are sufficient while for the more massive Ar^+ ions 3 layers (30 atoms) are needed.

In all the studies presented here, the incident primary ion has $E_0 = 600$ eV of energy and is at $\psi = 45°$ with respect to the surface in the $[1\bar{1}0]$ or $\phi = 0°$ direction (fig. 1). To compare with experimental conditions the ion must impact at all points on the surface, which by symmetry, is equivalent to impacting in the rectangular zone shown in fig. 1. For the ejection process we found that 50–100 trajectories or different impact points were sufficient to give reliable yields, cluster formation probabilities, angular distributions, and energy distributions of the ejected particles [9]. For the ion scattering calculations this number is not nearly sufficient. Initial scans of 2000–3000 trajectories were calculated for each type of ion. This many impact points are sufficient to identify regions of the impact zone that reflect the ion into various final scattering angles. To obtain statistically reliable energy distribution curves for a specific scattering angle, additional trajectories must be calculated in the appropriate impact regions, at a density equivalent to ~100,000 trajectories over the entire impact zone.

There is an alternate procedure to calculating a tremendous number of trajectories. Since the scattering angles and energies vary smoothly as a function of the impact points, it is possible to interpolate the values from the initial scan of about 2000 trajectories to a much denser grid. In this work both procedures have been employed. After the initial scan, an additional 1000 trajectories were calculated in 4% of the impact zone and then these were interpolated to an equivalent density of ~100,000 points over the entire impact zone.

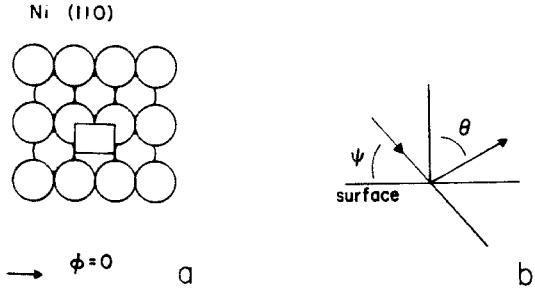

Fig. 1. Ni(110). (a) Crystal size; the impact zone is denoted by the rectangle. The ion is incident in the $[1\bar{1}0]$ or $\phi = 0°$ direction. (b) The scattering angles as used in the text.

Table 1
Potential parameters

	A (keV)	B (Å^{-1})	R_a (Å)
He^+–Ni	7.65	4.593	2.48
Ne^+–Ni	38.24	4.593	2.48
Ar^+–Ni	68.84	4.593	2.48

The interaction among the particles is assumed to be pairwise additive. The pair potential for the Ni–Ni interaction consists of three parts, a repulsive Born–Mayer function for small internuclear separations, an attractive Morse potential at long range, and a cubic spline to connect the two. The exact form and the parameters are given elsewhere [9g]. The interaction of the incident ion (He^+, Ne^+ or Ar^+) with Ni is represented by a purely repulsive function,

$$V = A\, e^{-BR}, \quad R < R_a,$$
$$V = 0, \quad R > R_a. \tag{1}$$

where V is the pair potential between the ion and the nickel separated by a distance R.

We have chosen to keep the potential parameters consistent with our recent studies of the particle ejection process [9d,g]. The parameter A in eq. (1) is scaled to the product of the atomic numbers of the two species similar to the screened Bohr form of potential interaction. The parameters for eq. (1) are given in table 1.

The trajectory is terminated when the primary ion has reflected and no longer interacts with the solid or when the ion implants with less than 5 eV of energy. The final velocity vector of the ion is analyzed for scattering angles (θ, ϕ) and energy (E). To determine an angular or energy distribution the resolution of the experiment must be specified. In the calculations the energy resolution is 10 eV while the angular resolution varies from 2–10°. We have used the polar angle θ as measured from the surface normal and the angle ϕ to represent the azimuthal direction. The relative orientations are shown in fig. 1b.

3. Results and discussion

The full molecular dynamics approach to the ion scattering process allows one to analyze for many observables including reflection (or alternatively, implantation), energy distribution and angular distribution of the primary ion. For a preliminary overview of the results of ~2000–3000 trajectories, the observables are displayed in contour plots (figs. 2–5) over the impact zone shown in fig. 1. The upper part of each frame in figs. 2–5 corresponds to the ion striking the first layer or ridge atoms

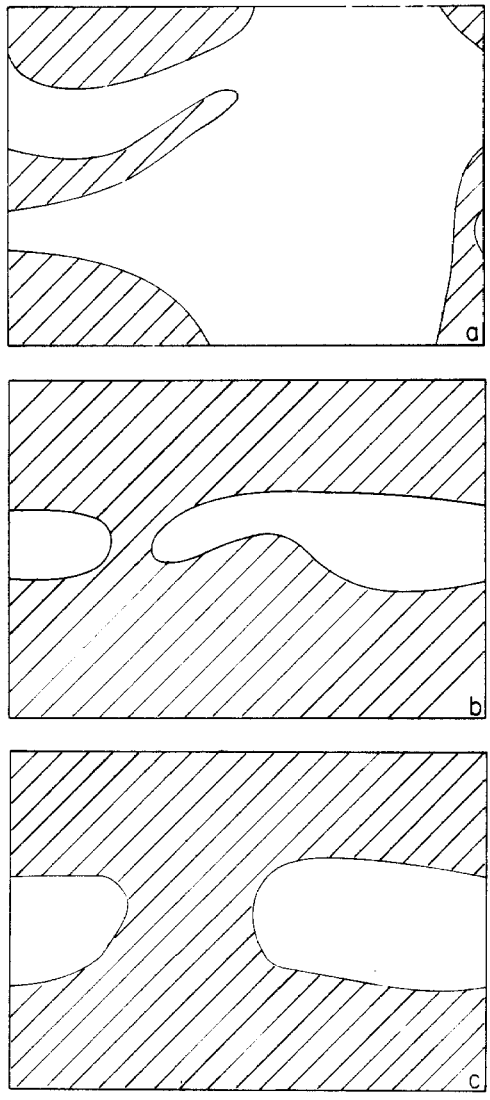

Fig. 2. Reflection and implantation. Each frame is the impact zone shown in fig. 1. The shaded region corresponds to reflection of the primary ion, while the unshaded region to implantation of the primary ion. (a) He^+, (b) Ne^+, (c) Ar^+.

of the (110) face. (Compare with the impact zone shown in fig. 1.) Similarly, the lower part of each frame corresponds to the ion impacting the second layer or valley atoms.

Care must be exercised when comparing the contours in the impact zone to the

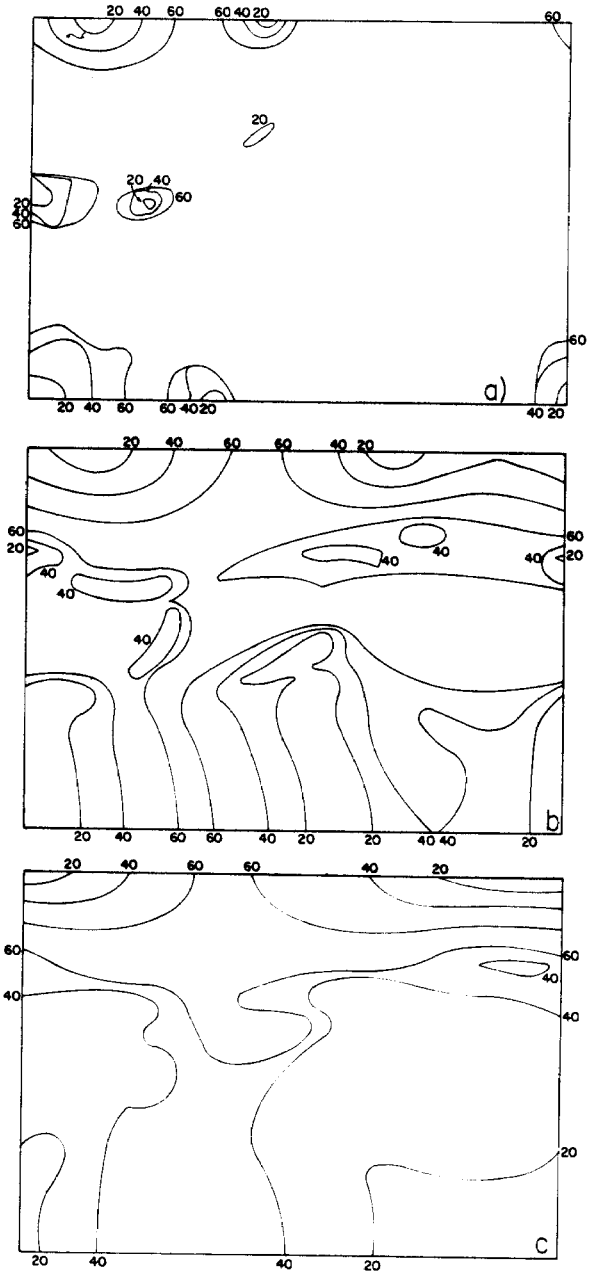

Fig. 3. Polar angle θ. The contours are at a constant final polar scattering angle of the primary ion. The numbers are the value of θ in degrees. (a) He^+, (b) Ne^+, (c) Ar^+.

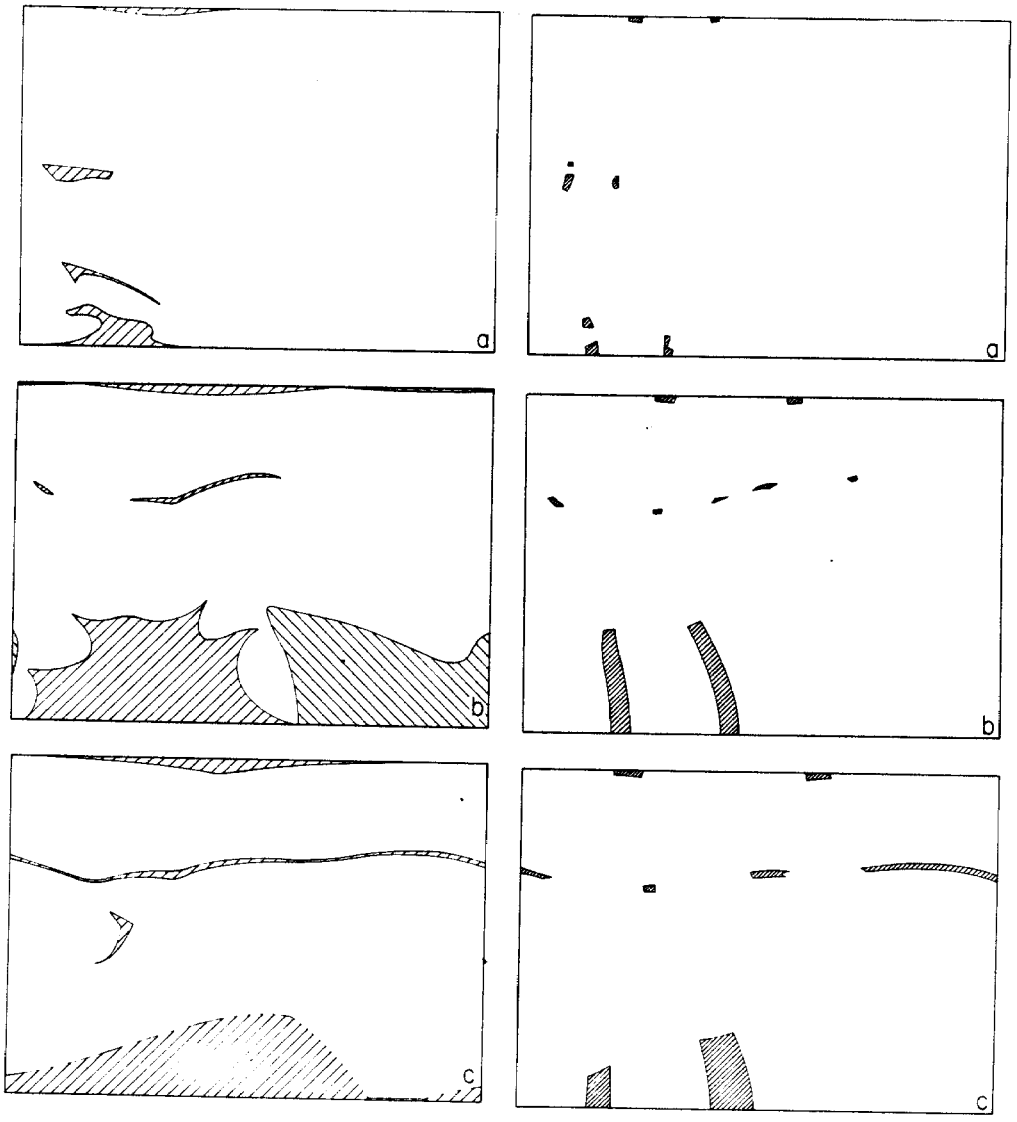

Fig. 4. Inplane scattering. The shaded areas are the impact regions where the ion scatters within $\pm 5^\circ$ of the in-plane direction. (a) He^+, (b) Ne^+, (c) Ar^+. The forward diagonal slashes are for $\phi = 0 \pm 5^\circ$ which occurs for all of the ions. Also shown are the impact regions for Ne^+ where the scattering is at $\phi = 180 \pm 5^\circ$. These latter regions are denoted by backward diagonal slashes.

Fig. 5. The shaded regions correspond to the ion scattering into the final angles of $\theta = 45 \pm 5^\circ$ and $\phi = 0 \pm 7^\circ$. (a) He^+, (b) Ne^+, (c) Ar^+.

placement of the atoms on the surface. The impact zone would contain the actual impact points of the incident ions, if the surface were *hard* and *flat*. However, the surface has structure and since the ion is incident from left to right at an angle of $\psi = 45^\circ$ with respect to the surface, the ion actually initially strikes the surface to the left of the impact point.

The regions that are shaded in fig. 2 show where the different primary ions reflect. For Ne^+ and Ar^+ reflection occurs primarily when the ion hits along the ridge or valley (1st or 2nd layer Ni atoms). The Ar^+ reflects ~75% of the time while the Ne^+ reflects ~80% of the time. Since the He^+ is considerably smaller than the other ions, it penetrates the lattice more easily. In fact the He^+ reflects only ~30% of the time. For all the ions there is a considerable amount of reflection from the second layer atom of the solid.

The polar angle, θ, contours are displayed in fig. 3. The curves for the three ions are quite similar. There are two sets of concentric "circles" along the first layer ridge, most dramatically seen in the He^+ contour plot, fig. 3a. The left set corresponds to what is referred to as the "single" collision region. By tracing the path and interactions of the ion for these impact points we find that the ions do, in fact, interact primarily with only one solid atom. The interactions with other solid atoms are quite small. As a measure of the collision strength use the largest mutual potential energy between the two colliding atoms. In the case of Ar^+ it experiences a 250–300 eV "binary" collision with one of the Ni atoms. The collisions with other surface atoms are generally less than 10 eV. For Ne^+ the collision with the main Ni atom is ~350 eV with the other collisions being at most ~2 eV.

The second set of concentric lines corresponds to the "double" scattering. Here the ion primarily interacts with two of the ridge atoms. Here the collisions are not binary or separable. For example, the Ar^+ strikes the first Ni atom with 150 eV collision, then simultaneously interacts in a 15–30 eV collision with each of two Ni atoms, finally striking the 2nd Ni atom with ~150 eV collision. An analogous set of contours are observed where the ion strikes the second layer atoms. Here, although the ion may primarily strike one or two of the second layer atoms many of the first layer atoms interact almost continuously with the primary ion. There are two sets of contours along the valley which are analogous to the "single" and "double" scattering along the ridge. In fact, the first layer atoms are responsible for channeling the ion along the incident direction.

Most ISS experiments only measure inplane scattering, that is, the plane of the incident and reflected ions is perpendicular to the surface. Thus, shown in fig. 4 are the impact regions that give rise to scattering within 5° of the inplane direction. There are two primary regions that lead to scattering in this direction: one along the ridge and the other along the valley. It is difficult for the ion to maintain its "balance" along the ridge which is the reason why this region is small. Along the valley the ion is channeled by the first layer atoms and the impact region which gives rise to inplane scattering is large. The effect has been labeled "surface semichanneling" [1,10]. There is a small region in the center of the impact zone which

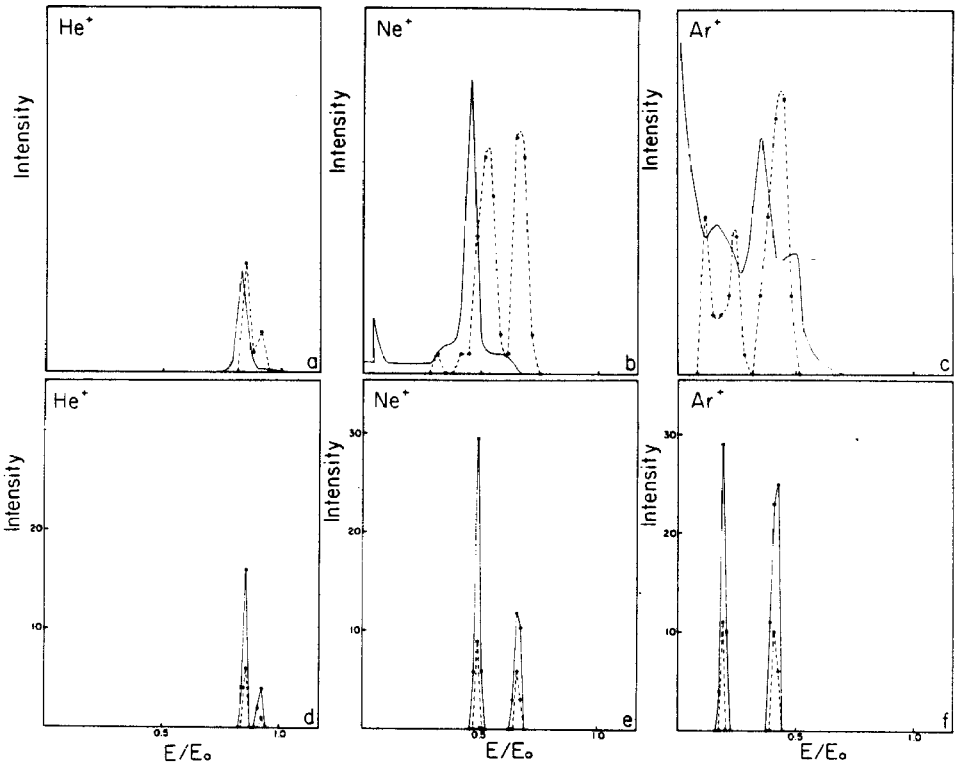

Fig. 6. Energy distributions. The intensity of ions scattered into a final angle are plotted versus E/E_0. The calculated curves in frames a–c include all particles that reflected inplane (see fig. 5): (———) experimental from ref. [8]; (– – –) calculated, $\theta = 45 \pm 5°$, $\phi = 0 \pm 7°$. The calculated curves in frames d–f include only ions that scatter from the first layer or ridge atoms: (———) calculated, $\theta = 45 \pm 2°$, $\phi = 0 \pm 2.8°$; (– – –) calculated, $\theta = 45 \pm 1°$, $\phi = 0 \pm 1.4°$.

also gives rise to inplane scattering. Analysis of these mechanisms shows that the ion "zig-zags" back and forth in the valley.

To compare with the experiments of Heiland and Taglauer [8] we have calculated energy distributions at a polar angle of 45° for inplane scattering. For the calculated distribution we have chosen an angular resolution of $\theta = 45 \pm 5°$ for the polar angle and $\phi = 0 \pm 7°$ for the inplane angle. Shown in fig. 5 are the impact regions that give rise to these particular observation angles. In figs. 6a–6c are the corresponding experimental and calculated energy distribution curves. These energy distributions do not agree very well with the experimental ones. To understand this further one must analyze the mechanisms contributing to the energy distribution curve.

Each region outlined in fig. 5 generally corresponds to a unique collision mecha-

Table 2
Sample collision times for He^+, Ne^+ and Ar^+ scattering from Ni(110) [a]

	He^+	Ne^+	Ar^+
"Single" collision from a first layer Ni atom	2.4 [b]	4.1	6.7
	(1.0) [c]	(1.0)	(1.0)
"Double" collision from first layer Ni atoms	3.2	5.8	8.3
	(1.3)	(1.4)	(1.2)
Collision from a second layer Ni atom [d]	4.4	10.1	16.1
	(1.8)	(2.5)	(2.4)
Collision from second layer Ni atoms [d]	5.5	11.0	17.4
	(2.3)	(2.7)	(2.6)

[a] The times reported are the total collision time as calculated from the trajectory. The actual time that the ion is interacting with the solid and is capable of being neutralized may be shorter.

[b] The times are given in femptoseconds (10^{-15} sec).

[c] Time of collision normalized to the time for a "single" collision from a first layer atom. Each primary ion has been normalized individually.

[d] Two different mechanisms of collision from second layer atoms. The mechanisms are approximately "single" and "double" scattering (see text).

nism, and thus the energy transfer is approximately constant over the region. Therefore, the larger the impact region in fig. 5, the more it contributes to a peak in the energy distribution curve. The second layer scattering is dominating the energy distribution curve. The ions that strike the second layer, however, interact with the solid approximately 2–3 times longer than the ions that impact along the ridge (table 2). It has been postulated that the probability of an ion surviving and not being neutralized, $P(\text{ion})$, is

$$P(\text{ion}) = A\, e^{-t/\tau},$$

where t is the interaction or collision time with the solid, τ is a lifetime and A is a constant [11]. For a rough approximation we have assumed that τ for each ion is the collision time of the "single" collision trajectories along the ridge. This implies that the ions reflected from the first layer have an 8–20 times larger probability of remaining as ions. The contribution of the second layer collisions to the energy distribution curve must be attenuated by a factor of 8–20.

To analyze the scattering from only the ridge region, an additional 800 impact points were evaluated in 4% of the impact zone. As discussed in section 2 the observables from these calculated points can be interpolated. By interpolating the points, we obtained 3200 points in this select region which corresponds to a density of over 80,000 impact points in the entire zone.

The energy distributions from only the first layer impact points are shown in

figs. 6d–6f. Two angular resolutions, indicated in the figure caption, are given. The agreement between the calculations and the experiments is noticeably better. For Ne^+ the improvement is most dramatic. In fig. 6b the two peaks in the calculated distribution are completely in the wrong positions and have approximately the same intensity. By attenuating out the contribution to the curve from the second layer collisions, fig. 6e, the peak and shoulder are at approximately the same positions as the experimental curve. Since the higher energy peak predominantly corresponds to collisions with at least 2 solid atoms, the time the ion spends near the surface is ~1.4 longer than the ions contributing to the peak at the lower energy. Thus the shoulder peak should probably be attenuated by a factor of ~4 with respect to the main peak. Other workers have shown that thermal effects will broaden the peaks and shift them to slightly lower energies [12]. In a recent paper by Luitjens, Algra, and Boers, they have examined 10 keV Ne^+ scattering from Cu(001) and analyzed for both the reflected Ne^+ ions and neutral Ne atoms [13]. They observe that the ratio of the multiple scattering peak intensity to single scattering peak intensity is larger for the neutral particles than the ions, as is observed in the comparison of the calculated results figs. 6d–6f, which include both ions and neutrals, with the experimental ion distributions.

The least dramatic changes are seen in the He^+ energy distributions (figs. 6a and 6d). Since the He^+ is so light compared with the substrate virtually all collisions yield the same final energy for the He^+ and it is difficult to distinguish the energy distributions with and without the second layer effects. Analysis of the individual trajectories, however, indicate that the second layer collisions also take ~2 times longer (table 2) than the first layer collisions and should be attenuated as in the case of Ne^+. The peaks in the experimental Ar^+ energy distribution display the most broadening, probably due to thermal motions of the substrate [1,12,14]. Since our model does not yet include thermal effects it is difficult to say whether the calculated curve in fig. 6c or fig. 6f reproduces the experimental one the best. However, since for the Ar^+ the second layer collision times are 2–3 times longer than the first layer collision times, it is only logical that a similar attenuation procedure must be followed for Ar^+ as well as He^+ and Ne^+. The relative probabilities of He^+, Ne^+ and Ar^+ will also depend on the details of the electronic structure of each ion and the substrate.

Thus we have found that the second layer scattering (or surface semi-channeling) contributes heavily to inplane reflection. For ion reflection, however, a correction must be made for the possibility of neutralization. Making this adjustment indicates that only first layer scattering contributes to the observed ISS energy distribution curves. This is in contrast with the work of Shulga et al. [10] who show that surface semi-channeling is important to describe the angular distributions of 4.5 keV Ar^+ ions from a Cu(100) crystal. The 4.5 keV ions spend less time interacting with the substrate, even for second layer collisions, and surface semi-channeling could occur.

The effect of angular resolution on the energy distribution curves is also shown

in figs. 6d–6f. As the angular resolution is improved the energy distribution peaks become sharper. Of particular note is that as the angular resolution of the analyzer is improved, the impact zones which lead to reflection of particles into its acceptance zone become smaller. This observation implies that the mechanisms of energy transfer are nearly identical within a given zone and that the resulting energy dispersion about a particular value will decrease. Even though the calculated resolution

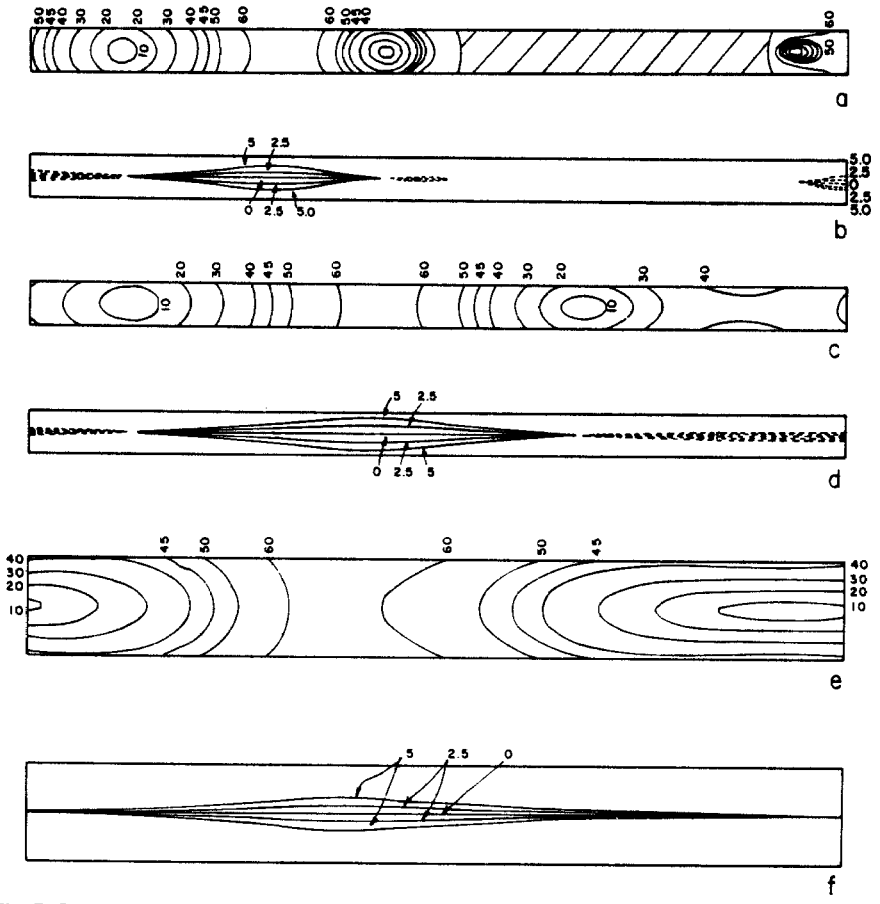

Fig. 7. Scattering angle contours for first layer scattering only. The impact zone has been reflected to include both sides of the first layer atoms thus there is a horizontal line of symmetry. Frames a–d represent ~4% of the impact zone shown in fig. 1, while frames e, f are ~8% of the impact zone. The final polar angle of the scattered ions is shown in frames a, c and e for He^+, Ne^+ and Ar^+, respectively. In frame a the slash marks correspond to the region of implantation. The deflection angle from the inplane direction is displayed in frames b, d and f for He^+, Ne^+ and Ar^+, respectively. The solid lines are deflections from the $\phi = 0°$ direction and the dashed lines are deflections from the $\phi = 180°$ direction. All numerical values are in degrees.

is different from the experiment, the peaks occur at the same positions.

Contours for the polar deflection angle of only the first layer region of the impact zone are shown in figs. 7a, 7c and 7e. The contours are evenly spaced in 10° intervals except for a contour at 45°. There is a maximum angle $\gtrsim 60°$ into which scattering can occur. The impact region which corresponds to this angle is located at the point where the concentric circles of the "single" scattering mechanism merge with the "double" scattering lines. The maximum angle is observed experimentally [1]. This angle is commonly called the rainbow angle particularly in lower energy scattering. (Note that if the polar angle is measured from the forward direction this corresponds to a minimum total scattering angle.) The spacing between the contour lines is largest near the classical rainbow angle. Since there is a large impact region scattering into one angle, the intensity of scattering ions greatly increases. This relationship is illustrated in fig. 8 by plotting the polar angular distribution for the first layer scattering. The rainbow structure is very apparent for all the ions as evidenced by a maximum in intensity at ~65° for all the species. This increase in intensity is due to two factors. First, as discussed above, there is a large impact region which scatters ions into the rainbow angle. Second, as seen in figs. 7b, 7d and 7f, the region of the impact zone that scatters the ions inplane also increases at the rainbow angle. Thus, to determine the scattering intensity as a function of angle, even for inplane scattering, a full three-dimensional calculation needs to be performed.

Since predominantly only one mechanism gives rise to scattering into the rainbow angle, the energy distribution should contain only one peak. As shown in fig. 9, this prediction is indeed correct. As the collision times are approximately the same as for the cases shown in figs. 6d–6f, the same intensity scales are used. The case of Ar^+ is somewhat anomalous in that the maximum angle (fig. 9e) does not have the maximum intensity. Shown in fig. 9c are the energy distributions for $\theta = 60°$ (maximum total intensity) and $\theta = 65°$ (maximum angle). The two peaks merge as the scattering mechanisms become unique.

The actual position of the rainbow angle depends on the roughness of the surface as perceived by the ion and the lattice spacing as well as the angle of incidence of the primary ion. Thus one would not expect the same rainbow angles for scattering from the first and second layers. This expectation is hinted at in the contour plots of fig. 3.

Although we have been analyzing only the ions that reflect in the forward inplane direction, some of the ions reflect and completely turn around. This phenomenon is only observed for the Ne^+ and He^+ scattering. Figs. 4b, 7b and 7d display the impact regions that give rise to inplane scattering in the reverse direction ($\phi = 180°$). These ions also exhibit a rainbow angle, see fig. 8. The impact regions that scatter the ions at $\phi = 180°$ are smaller than the regions for $\phi = 0°$. In addition, the collision times of ions that scatter from the ridge into $\phi = 180°$ are ~2 times longer than collision times of ions that scatter from the ridge into $\phi = 0°$. Both of the factors contribute to a lower intensity for scattering at $\phi = 180°$ than $\phi = 0°$. As in the

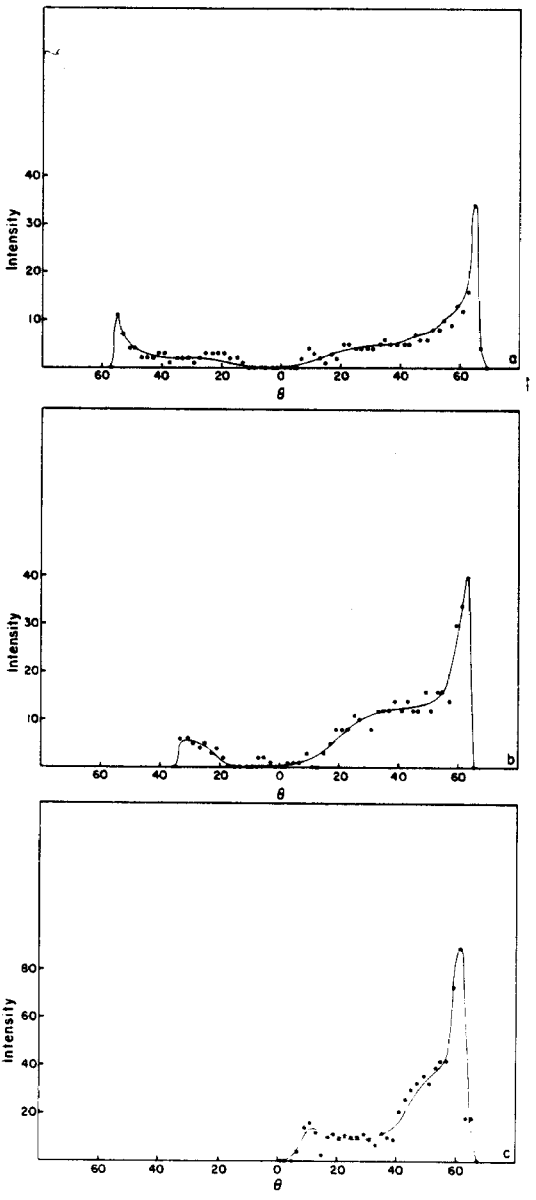

Fig. 8. Rainbow angles. The inplane scattering intensity is plotted versus the polar angle, θ. Angles to the right of $\theta = 0^\circ$ on the graph correspond to $\phi = 0^\circ$ while angles to the left are for $\phi = 180^\circ$. (a) He^+, (b) Ne^+, (c) Ar^+.

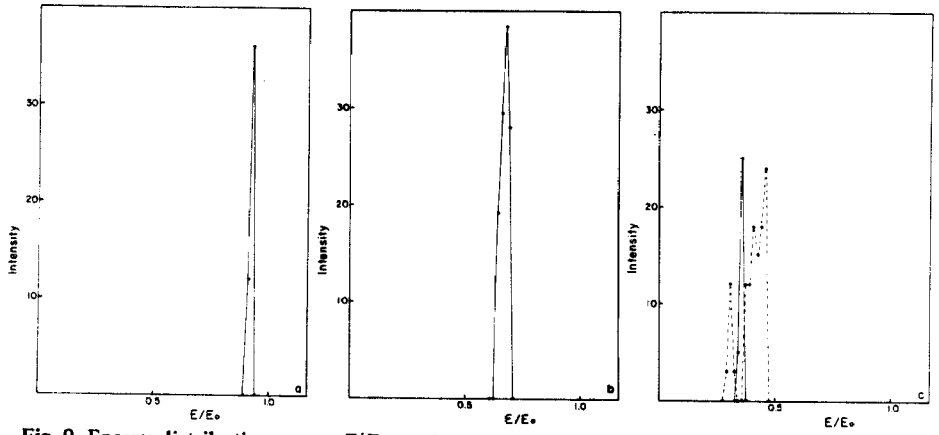

Fig. 9. Energy distribution versus E/E_0 at the rainbow angle. The curves include only ions scattered from the first layer or ridge atoms. The angular resolution and the intensity scale is the same as the dashed curves in figs. 6d–6f. (a) He^+; $\theta = 66 \pm 1^\circ$, $\phi = 0 \pm 1.4^\circ$. (b) Ne^+; $\theta = 62.5 \pm 1^\circ$, $\phi = 0 \pm 1.4^\circ$. (c) Ar^+; (———) $\theta = 65 \pm 1^\circ$, $\phi = 0 \pm 1.4^\circ$; (– – –) $\theta = 60 \pm 1^\circ$, $\phi = 0 \pm 1.4^\circ$.

case of scattering at $\phi = 0^\circ$, the second layer scattering at $\phi = 180^\circ$ predominates (fig. 4b).

4. Conclusions

We have presented a full three-dimensional calculation of the scattering of He^+, Ne^+ and Ar^+ ion beams from the (110) face of nickel. The incident ion has an energy $E_0 = 600$ eV at $\psi = 45^\circ$ in the $[1\bar{1}0]$ direction. The energy distributions of the reflected primary ions have been compared to the experimental results of Heiland and Taglauer [8].

We find that the majority of the inplane scattering arises from the primary ion reflecting off the second layer or valley atoms of the solid. However, the times of these collisions are 2–3 times longer than collisions of the primary ion with the first layer atoms. The longer collision times result in a larger probability of the ion being neutralized. Thus the contribution of second layer collisions to the energy distribution curve must be attenuated. This attenuation results in better agreement between the calculated energy distributions and the experimental ones.

We find that for the "single" collisions with the first layer or ridge atoms the scattering process is a binary collision. For the "double" scattering along the ridge and all second layer collisions the primary ion interacts with more than one atom of the solid at a time. The binary collision model is not a valid approximation for the vast majority of the collisions. Thus for experiments that rely on shadowing to predict surface structure, the binary model is in most cases appropriate. However, for

experiments which are measuring surface concentration, neutralization of the primary ion or second layer scattering effects, a full calculation is necessary.

To describe the intensity of the scattered primary ion at a given angle we have found that a three-dimensional calculation is necessary. The scattered intensity increases at the rainbow angles not only due to a large region of the impact zone scattering at the appropriate polar angle but the impact region corresponding to inplane scattering also increases.

The model presented in this study describes the scattering of ions from a clean metal surface. The probability of the ion being neutralized is included. This model provides a basis for incorporating thermal effects and for studying systems such as alloys and adsorbates.

Acknowledgements

This research was supported in part by the National Resource for Computation in Chemistry under a grant from the National Science Foundation and the Basic Energy Sciences Division of the United States Department of Energy under Contract No. W-7405-ENG-48. The portions of the computations done at the Purdue University Computing Center were supported by the Presidents Reserve Fund. Helpful discussions with N. Winograd are also acknowledged.

References

[1] A review of most experimental and theoretical work is given by E.P.Th.M. Suurmeijer and A.L. Boers, Surface Sci. 43 (1973) 309.
[2] P. Sigmund, Phys. Rev., 184 (1969) 184.
[3] See for example, E.S. Parilis, in: Proc. 7th Intern. Conf. on Phenomena in Ionized Gases, Belgrade, 1965, p. 129, and the references cited in ref. [1].
[4] See, for example, E.S. Parilis and N.Yu. Turaev, Soviet Phys.-Dokl. 10 (1965) 212;
E.S. Mashkova and V.A. Molchanov, Soviet Phys.-Dokl. 12 (1967) 133;
E.S. Mashkova, V.A. Molchanov and Soshka, Phys. Status Solidi 19 (1967) 425, and the references cited in ref. [1].
[5] See, for example, V.M. Kivilis, E.S. Parilis and N.Yu. Turaev, Soviet Phys.-Dokl. 12 (1967) 328, and the references cited in ref. [1].
[6] See for example, D.S. Karpuzov, V.A. Eltekov and V.E. Yurasova, Soviet Phys.-Solid State 8 (1967) 1726;
V.E. Yurasova, V.I. Shulga and D.S. Karpuzov, Can. J. Phys. 46 (1968) 759, and the references cited in ref. [1].
[7] D.S. Karpuzov and V.E. Yurasova, Phys. Status Solidi (b) 47 (1971) 41.
[8] W. Heiland and E. Taglauer, J. Vacuum Sci. Technol. 9 (1971) 620.
[9] (a) D.E. Harrison, Jr., P.W. Kelly, B.J. Garrison and N. Winograd, Surface Sci. 76 (1978) 311.
(b) B.J. Garrison, N. Winograd and D.E. Harrison, Jr., J. Chem. Phys. 69 (1978) 1440.
(c) N. Winograd, D.E. Harrison, Jr. and B.J. Garrison, Surface Sci. 78 (1978) 467.

(d) B.J. Garrison, N. Winograd and D.E. Harrison, Jr., Phys. Rev. B18 (1978) 6000.
(e) N. Winograd, B.J. Garrison, T. Fleisch, W.N. Delgass and D.E. Harrison, Jr., J. Vacuum Sci. Technol. 16 (1979) 629.
(f) B.J. Garrison, N. Winograd and D.E. Harrison, Jr., J. Vacuum Sci. Technol. 16 (1979) 789.
(g) N. Winograd, B.J. Garrison and D.E. Harrison, Jr., Phys. Rev. B, submitted.
[10] V.I. Shulga, I.G. Bunin, V.E. Yurasova, V.V. Andreev and B.M. Mamaev, Phys. Letters 37A (1971) 181.
[11] The survival probability according to H.D. Hagstrom, in: Electron and Ion Spectroscopy Solids, Eds. L. Fiermans, J. Vennik and W. Dekeyser (Plenum, New York, 1978), is expressed in terms of velocity. Here it has been rewritten in terms of time since the distance traveled for all ions is approximately equal.
[12] E.S. Parilis, N.Yu. Turaeu and V.M. Kivilis, in: Proc. 8th Intern. Conf. on Phenomena in Ionized Gases, Vienna, 1967), p. 47.
[13] S.B. Luitjens, A.J. Algra, and A.L. Boers, Surface Sci. 80 566 (1979).